Investigation of the reaction mechanisms for $^{10}B + ^{197}Au$ at near-barrier energies

L. R. Gasques,[1] L. C. Chamon,[1] A. Lépine-Szily,[1] V. Scarduelli,[1] V. A. B. Zagatto,[2] D. Abriola,[3] A. Arazi,[3] M. A. Cardona,[3] E. de Barbará,[3] J. de Jesús,[3] D. Hojman,[3] G. V. Martí,[3] A. J. Pacheco,[3] D. Ramos López,[3] M. A. G. Alvarez,[4,5] J. P. Fernández-García,[4,5] M. Rodríguez-Gallardo,[4,5] M. Cubero,[6] L. F. Umaña,[6] and S. Achí-Prado[7]

[1]*Universidade de Sao Paulo, Instituto de Fisica, Rua do Matao, 1371, 05508-090 Sao Paulo, Sao Paulo, Brazil*

[2]*Instituto de Física da Universidade Federal Fluminense, 24210-346 Niterói, Rio de Janeiro, Brazil*

[3]*Laboratorio TANDAR, Comisión Nacional de Energía Atómica, Av. Gral. Paz 1499, BKNA1650 San Martín, Argentina*

[4]*Departamento de Física Atómica, Molecular y Nuclear, Facultad de Física, Universidad de Sevilla, Apartado 1065, E-41080 Sevilla, Spain*

[5]*Instituto Carlos I de Física Teórica y Computacional, Universidad de Sevilla, Spain*

[6]*Escuela de Física, Universidad de Costa Rica, 11501-Apdo. 2060, San José, Costa Rica*

[7]*Centro de Investigación en Ciencias Atómicas, Nucleares y Moleculares, Universidad de Costa Rica, 11502-Apdo. 2060, San José, Costa Rica*

(Received 29 November 2019; revised manuscript received 10 March 2020; accepted 20 March 2020; published 13 April 2020)

The $^{10}B + ^{197}Au$ reaction has been investigated through cross-section measurements for different channels, such as quasielastic and elastic scattering, inelastic excitation of low-lying ^{197}Au states, and one-neutron pickup and one-proton stripping transfer reactions. Experimental angular distributions were obtained for 20 bombardment energies around the Coulomb barrier: $38 \leqslant E_{lab} \leqslant 61$ MeV. Coupled reaction channels calculations have been performed in the context of the double-folding São Paulo potential, and details of the data analysis are discussed along the paper. In general, the theoretical calculations provide a satisfactory description of the data.

DOI: 10.1103/PhysRevC.101.044604

I. INTRODUCTION

Despite a century of important discoveries, our understanding of the mechanisms and dynamics of nuclear reactions has many important gaps. Atomic nuclei are complex many-body systems governed by the laws of quantum mechanics, and a significant number of important questions regarding the structure of the nuclei still have to be addressed. Low-energy collisions have often been used to study the dynamics of the nuclear reactions and the bulk properties of several nuclear species and their interactions [1–3].

Rare-isotope beam facilities have opened a new era of opportunities for the study of exotic nuclei. The capability to produce radioactive beams far from the line of stability has allowed measurements of unprecedented relevance in nuclear physics. The low binding energy of protons or neutrons with the core may enlarge the probability of the nucleus breaking up in nuclear collisions. Measurements of fusion excitation function involving a Borromean halo nucleus have shown considerable enhancement of the fusion probability in comparison with coupled-channel theoretical predictions [4–6]. More recently, experiments aiming to investigate the role of cluster-transfer reactions have been performed with radioactive beams in inverse kinematics. The results have demonstrated that cluster-transfer reactions can be well described as a direct process, and thus they are an important tool to investigate the structure of radioactive neutron-rich nuclei [7–9]. However, the reaction mechanisms of systems involving light unstable weakly bound nuclei, such as $^{6,8}He$ or ^{11}Be, and stable weakly bound projectiles, such as $^{6,7}Li$ and ^{9}Be, can be extremely puzzling [10–15].

Although experimental and theoretical developments in the field of low-energy nuclear reactions with radioactive beams have been recently achieved, studies of systems involving stable weakly bound nuclei are often performed to disentangle competing reaction mechanisms [13–20]. To extend the investigation of the dynamics of nuclear reactions involving stable weakly bound nuclei, this paper presents experimental angular distributions for some $^{10}B + ^{197}Au$ reaction channels measured at several bombarding energies around the Coulomb barrier: $38 \leqslant E_{lab} \leqslant 61$ MeV.

The nucleus ^{10}B presents a breakup threshold of 4.461 MeV in the partition $^{6}Li + \alpha$, which, although higher than those of $^{6,7}Li$ and ^{9}Be α-cluster nuclei, is still significantly lower than the typical values of binding energies of strongly bound nuclei, including its isotope ^{11}B that has a $Q = 8.665$ MeV for breaking into $^{7}Li + \alpha$. Hence, it can be expected that the breakup can play an important role in the reaction mechanisms of ^{10}B [21,22]. However, measurements involving ^{10}B projectile have been less often explored in comparison with other weakly bound nuclei. In the present work, ^{197}Au was chosen as target since it allows the study of complete and incomplete fusion, one-neutron pickup and stripping processes via the offline detection of delayed γ rays [23]. On the other hand, for the sake of the study of elastic scattering, the choice of the target poses an experimental challenge because of the quite low excitation energies of its low-lying excited sates.

The data analyzes are performed within the context of the coupled reaction channel (CRC) theoretical formalism. The paper is organized as follows: The experiments are described

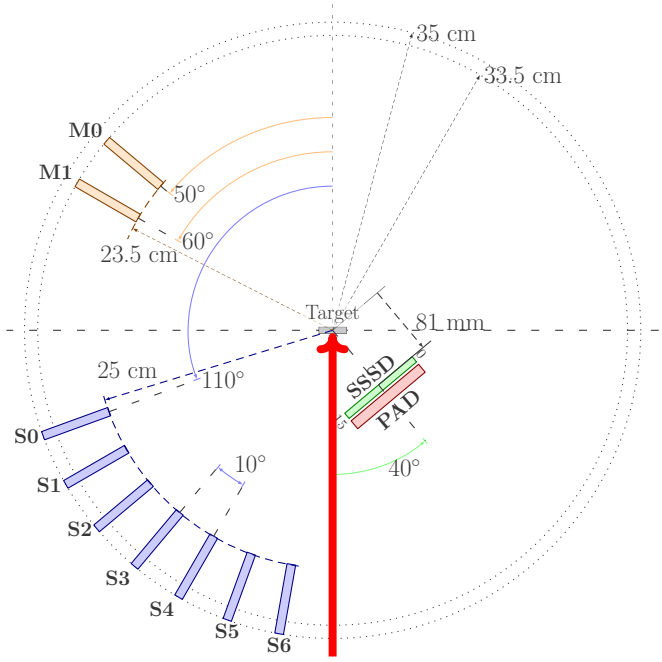

FIG. 1. Schematic view of the setup mounted at the 30B scattering chamber.

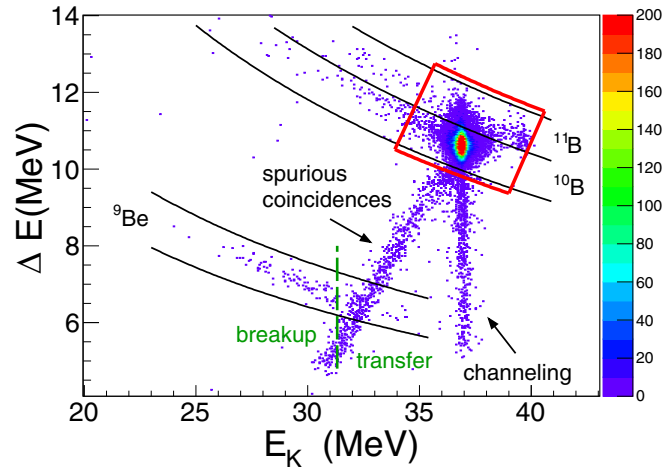

FIG. 2. $\Delta E - E_K$ spectrum obtained at $E_{lab} = 44$ MeV and $\theta_{lab} = 133^\circ$. The bands represent regions related to the detection of ^{10}B, ^{11}B, and ^{9}Be. The region of the quasielastic process is indicated in the figure by the red square. Arrows indicate regions of spurious coincidences and channeling. The dashed green line separates the regions associated to the one-proton stripping transfer and breakup processes related to the detection of ^{9}Be.

in Sec. II; experimental results are compared with theoretical predictions in Sec. III; and the main conclusions are presented in Sec. IV.

II. EXPERIMENTAL SETUP

The measurements involve a joint collaboration among research groups from Argentina, Brazil, Costa Rica, and Spain and were carried out in two laboratories. Part of the experiment was performed at the Institute of Physics of the University of São Paulo (USP), using the 8-MV Pelletron accelerator installed at the Open Laboratory of Nuclear Physics (LAFN, acronym in Portuguese), Brazil. Since the Coulomb barrier for $^{10}\mathrm{B} + {}^{197}\mathrm{Au}$ is about 50 MeV, it is not possible to take data for this system at energies above the barrier using the LAFN facility. Therefore, an extension of the energy range of the measurements was performed using the 20-MV tandem accelerator TANDAR (TANDem of ARgentina). The measurements at LAFN were performed at $E_{lab} = 38$, 40, 42, 44, and 46 MeV, while the measurements at $E_{lab} = 38$, 40, 42–45, 47–59, and 61 MeV were performed at the TANDAR Laboratory.

In the experiment performed at LAFN, the ^{10}B beam was focused on a target containing a thin layer of ^{197}Au (about $8\,\mu\mathrm{g/cm^2}$) evaporated onto a $10\,\mu\mathrm{g/cm^2}$ carbon backing. The very small ^{197}Au thickness is quite important to obtain sufficient energy resolution to separate the elastic peak from those corresponding to the inelastic excitation of the low-lying ^{197}Au states. A schematic view of the setup is shown in Fig. 1. Part of the experiment was performed with a set of single semiconductor silicon surface barrier detectors, giving information about the kinetic energy of the particle E_K. Other part was performed using $\Delta E - E_R$ telescopes (SSSD-PAD in the figure), where ΔE represents the energy loss of a particle in a thin barrier detector, while E_R is the remaining energy left in a thick detector.

Figure 2 presents a typical bidimensional $\Delta E - E_K$ spectrum obtained at $E_{lab} = 44$ MeV and $\theta_{lab} = 133^\circ$, where $E_K = \Delta E + E_R$. According to the results of energy-loss calculations, the bands shown in the figure represent regions expected for the detection of ^{10}B, ^{11}B, and ^{9}Be. The region of highest counting rate within the ^{10}B band corresponds to the elastic scattering process. In this same band, a region with events of ^{197}Au and/or ^{10}B inelastic excitation can be observed in the left side of the elastic scattering region. The ^{11}B band corresponds to the one-neutron pickup transfer reaction. Since $^{197}\mathrm{Au}(^{10}\mathrm{B}, {}^{11}\mathrm{B})\,{}^{196}\mathrm{Au}$ has a positive Q value of about 3.38 MeV for the ground state (g.s.), it is possible to observe, in the ^{11}B band, some events in the right side of the elastic region (i.e., ^{11}B nuclei with energy values larger than those of ^{10}B elastically scattered). There are also counts of ^{11}B in the left side of the ^{10}B elastic scattering that arise from one-neutron pickup populating states of ^{11}B and/or ^{196}Au with high excitation energy. Because of the high counting rate of the elastic process, it was not possible to separate ^{11}B from ^{10}B events in the energy region around the elastic scattering. Thus, we obtained one-neutron transfer cross sections in two regions of excitation energy: $0 \leqslant E^* \leqslant 1.8$ MeV and $4 \leqslant E^* \leqslant 8$ MeV.

Figure 2 also shows events within the ^{9}Be band. As discussed in the next section, part of these events are related to the one-proton stripping transfer and the other part to the breakup process. There is a region with counts originated by false events (spurious coincidences; see arrow in Fig. 2) starting from the elastic scattering and passing through the ^{9}Be region. We have estimated the contribution of these false events in order to correct the ^{9}Be cross sections. One can also

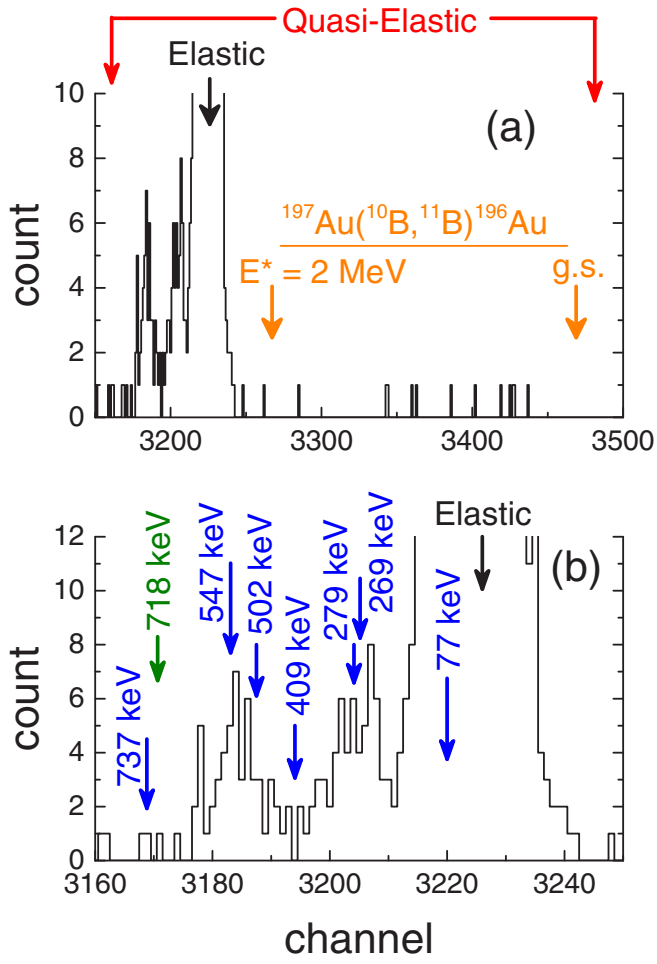

FIG. 3. Single channel spectrum taken at $E_{lab} = 46.0$ MeV and $\theta_{lab} = 130^{\circ}$. The energy regions corresponding to the quasielastic process, elastic scattering, and one-neutron pickup transfer (with $0 \leqslant E^* \leqslant 2$ MeV) are indicated in the top part of the figure. In the bottom, the arrows indicate the expected positions of peaks related to the elastic and inelastic (excitation of the first seven ^{197}Au and the first 718-keV ^{10}B low-lying states) processes.

observe in Fig. 2 a region containing events related to the channeling process [24]. The total counts related to the sum of spurious coincidence and channeling events represents a quite small fraction of about 2% of the elastic scattering yield. Even so, we have taken care to consider the channeling effect in the calculations of cross sections.

A typical spectrum of single detector taken at $E_{lab} = 46$ MeV and $\theta_{lab} = 130^{\circ}$ is shown in Fig. 3. In Fig. 3(a), we indicate the position of the peak corresponding to ^{10}B that comes from the elastic process. There are also some events related to the detection of ^{11}B from the one-neutron pickup process. The figure indicates a region corresponding to ^{196}Au excitation energies in the range $0 \leqslant E^* \leqslant 2$ MeV. For this region, the detected ^{11}B have kinetic energies larger than those for the ^{10}B elastically scattered and, therefore, they appear in the right side relative to the elastic scattering peak (in both Figs. 3 and 2). Because of this characteristic, it is easy to obtain the counts for neutron transfer in this excitation energy range, without any contamination by the quite intense elastic scattering process or inelastic excitation.

The arrows in the Fig. 3(b) indicate the expected positions of the peaks corresponding to the elastic scattering and inelastic excitation of the seven first ^{197}Au and the first (718-keV) ^{10}B low-lying states. The inelastic excitation of the 77-keV $1/2^+$ ^{197}Au state could not be separated from the elastic scattering. Thus, we name here as the "elastic" scattering cross section the sum of the contributions of the elastic process itself with the inelastic excitation of the 77-keV ^{197}Au state. We point out that our theoretical calculations indicate that the excitation of the 77-keV state presents very small contribution in comparison with that of the (pure) elastic scattering.

We have obtained cross sections for two groups of inelastic scattering: One is composed of the 269-keV $3/2^+$ and 279-keV $5/2^+$ states, and the other of the 502-keV $5/2^+$ and 547-keV $7/2^+$ states (see Fig. 3). According to our spectra, and also to our theoretical calculations, the cross sections for these two groups are much larger than that for the 409-keV $11/2^-$ state and also those for excitation energies larger than 700 keV. The energy (E_K) resolution of a bidimensional $\Delta E - E_K$ spectrum is worse than that for a single detector. Thus, the cross sections for the two groups of inelastic excitation were obtained only with the set of single detectors. However, it is not possible to separate (in energy) these two groups from the one-neutron transfer process (with high excitation energy) with single detectors. On the other hand, analyzes of the bidimensional spectra (where ^{10}B is separated from ^{11}B) indicate that the "contamination" is not much significant, since the counts of the neutron transfer are much smaller than those for the inelastic excitation. An inspection of Fig. 3(a) also indicates that the yield of neutron transfer is much smaller than that for inelastic excitation.

The inelastic scattering cross sections can reach up to about 10% of the elastic ones at $E_{lab} = 46$ MeV and 60% at $E_{lab} = 61$ MeV. Nevertheless, the high experimental energy resolution necessary to separate the elastic and inelastic processes is not reached in many cases. On the other hand, it is quite easy to obtain the total count of processes with energies around that of the elastic peak (see the region of red lines in Figs. 2 and 3). We define quasielastic cross section as the sum of the elastic scattering, inelastic excitation, and neutron-transfer cross sections in this condition. As the neutron-transfer cross section is very small, the quasielastic cross section is mostly determined by the sum of the elastic scattering with the two groups of inelastic excitation above commented. In the process of normalization of the experimental data, we have assumed that the quasielastic cross section is equal to the Rutherford cross section at $E_{lab} = 38$ MeV.

The detector system in TANDAR (see Fig. 4) comprises a rotating array of eight surface-barrier detectors (1 mm thick), with an angular separation of 5° between adjacent detectors, and two additional detectors usually kept at backward angles ($\theta_{lab} = 160^{\circ}$ and 168°). The detectors of the array were placed at 300 mm from the target and had collimators that defined angular acceptances smaller than 0.5° and solid angles between 0.12 and 0.8 msr. Two monitor detectors at $\theta_{lab} = \pm 16^{\circ}$ and a Faraday cup were used for normalization purposes. Self-supporting ^{197}Au targets with thicknesses of

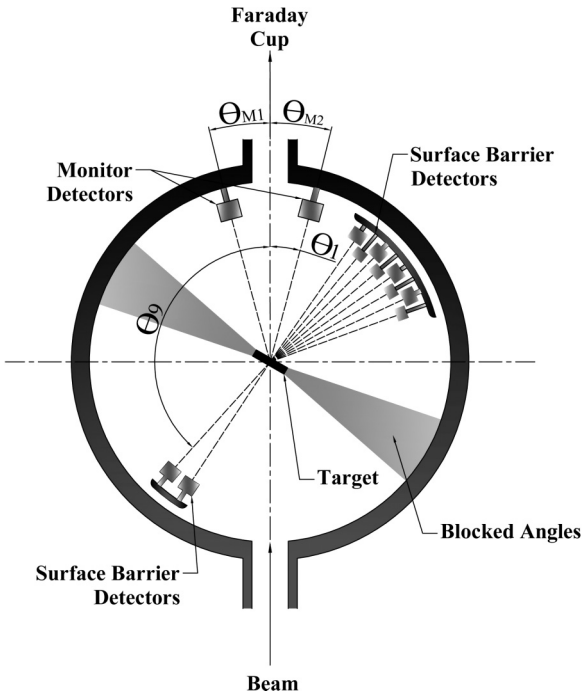

FIG. 4. Schematic view of the setup mounted at TANDAR.

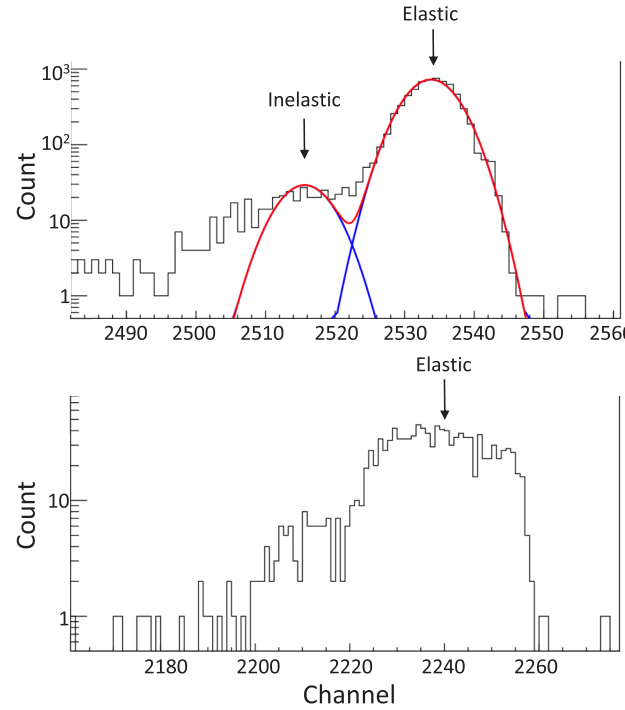

FIG. 5. Single-channel spectra obtained in TANDAR at $E_{lab} = 50$ MeV and $\theta_{lab} = 55^\circ$ (top) and $\theta_{lab} = 137^\circ$ (bottom).

about 250 μg/cm^2 were used at TANDAR. These targets, much thicker than those used at LAFN, resulted in high counting rates that also allowed the measurement of (complete and incomplete) fusion-evaporation by the offline detection of delayed γ rays (from the targets and aluminum catchers) [23]. However, the larger thickness resulted in a worse energy resolution in comparison with the one achieved at LAFN, in particular at backward angles for which the projectiles can have very different energy loss due to the corresponding different paths inside the target.

Figure 5 presents two single channel spectra obtained in TANDAR at $E_{lab} = 50$ MeV and $\theta_{lab} = 55^\circ$ (top of the figure) and 137° (bottom), with logarithmic scale in the ordinate axis. The arrows point the centroid of the elastic scattering peak and the bump produced by inelastic scattering corresponding to several excited states of ^{197}Au. In the backward angular region, the energy resolution is not enough to separate the elastic and inelastic processes and, thus, for this angular region we have obtained cross sections only for the quasielastic process. For forward angles, in addition to the quasielastic, it was possible to fit the peaks (as illustrated in the figure) and obtain reasonable estimates of cross sections for the elastic channel.

III. DATA ANALYSIS

The data were compared with theoretical CRC calculations using the FRESCO code [25]. In order to avoid ambiguities, we tried to fit the data with a minimum number of adjustable parameters that still provide a good description of the experimental results. The parameter-free São Paulo potential (SPP) [26] was adopted to describe the real part of the optical potential (OP). The imaginary part was assumed as proportional to the SPP,

$$U_{OP}(R) = V_{SPP}(R) + i\,N_I\,V_{SPP}(R), \tag{1}$$

where N_I was considered as an energy-independent adjustable parameter. The SPP predicts an s-wave barrier height of $V_B = 47.1$ MeV (49.5 MeV in the laboratory frame of reference), and we have obtained experimental angular distributions in the energy range of $38 \leqslant E_{lab} \leqslant 61$ MeV.

Since the ^{10}B g.s. has spin 3^+, we have also included a real spin-orbit potential in the central part of the optical interaction, with a form factor corresponding to the derivative of a Woods-Saxon shape. The respective reduced radius and diffuseness values were fixed at $r_0 = 1.06$ fm and $a = 0.6$ fm. The (energy-independent) strength V_0 was adjusted to fit the data.

Table I presents parameter values (obtained from Refs. [27,28] and references therein) related to the couplings of inelastic excitation channels. The nuclear deformation (δ)

TABLE I. Values of parameters involved in the inelastic couplings of excited states to the g.s. of the ^{197}Au or ^{10}B nuclei.

Nucleus	spin	E^* (MeV)	$M(E2)$ (fm^2)	δ (fm)
^{10}B	1^+	0.718	3.5	1.22
^{197}Au	$1/2^+$	0.077	69	0.59
^{197}Au	$3/2^+$	0.269	71	1.30
^{197}Au	$5/2^+$	0.279	118	0.61
^{197}Au	$5/2^+$	0.502	53	0.46
^{197}Au	$7/2^+$	0.547	141	1.02

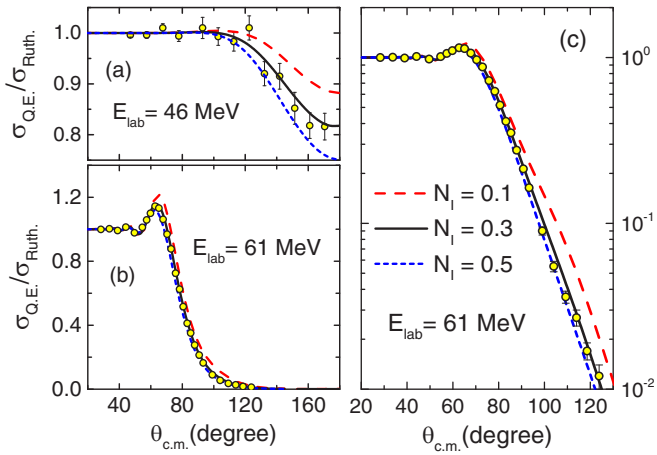

FIG. 6. Experimental quasielastic angular distributions for $E_{lab} = 46$ and 61 MeV. The lines represent CRC results for different N_I values. Note the change from linear (a) to logarithmic (b) scale.

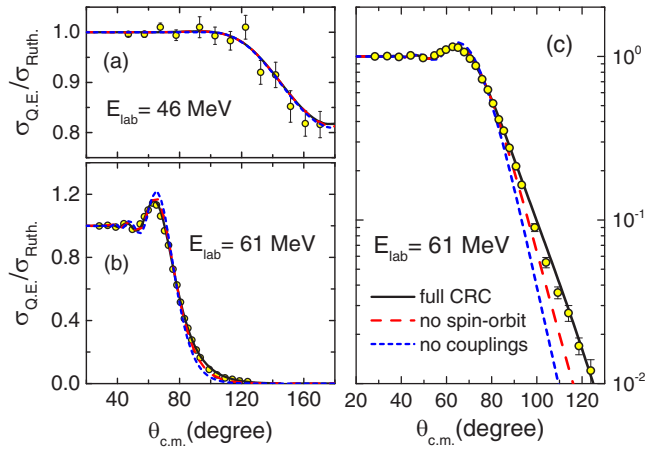

FIG. 7. Experimental quasielastic angular distributions for $E_{lab} = 46$ and 61 MeV. The solid black lines represent the results of the full CRC calculations, the dashed red lines show those obtained by turning off the spin-orbit interaction, while the dotted blue ones represent optical model calculations, using $N_I = 0.30$ in Eq. (1) for the optical potential.

was obtained from the Coulomb transition parameter taking into account the correction due to the finite diffuseness value of the nuclear densities [29]. These excited states were coupled directly to the corresponding g.s. (^{197}Au or ^{10}B) through the quadrupole mode ($\lambda = 2$). We have verified that couplings of second order to these states and also couplings to other states with higher excitation energies do not provide significant contributions for the cross sections of channels for which we have experimental angular distributions. We have also verified that the reorientation of the ^{197}Au g.s., with quadrupole moment of $Q = 594$ fm^2 [30], provides a contribution of about 20% for the quasielastic cross section, only for high energies and backward angles.

In Fig. 6, we illustrate the effect of N_I on the quasielastic data fit. The figure shows experimental and CRC theoretical results for $E_{lab} = 46$ MeV (below the barrier) and $E_{lab} = 61$ MeV (above the barrier) for three N_I values. Note the change from linear (a) to logarithmic (b) scale. Considering the results for all energies of this work, we have found the following best data fit value: $N_I = 0.30$. A similar value has also been obtained in the case of ^{10}B + ^{120}Sn [19,20].

In Fig. 7, we show the effects of the couplings and spin-orbit interaction on the quasielastic cross sections, for the same energies $E_{lab} = 46$ and 61 MeV. The solid black lines in this figure represent the results of the full CRC calculations (with $N_I = 0.30$), the dashed red lines were obtained turning off the spin-orbit interaction, while the dotted blue ones are the results of optical model (no couplings) calculations (also without spin orbit). The couplings and the spin-orbit potential do not make any difference for low energies, but are important to account for the data in the high-energy region. Our analysis resulted in the following best data-fit value for the strength of the spin-orbit interaction: $V_0 = 6$ MeV.

A. Elastic and quasielastic processes

Figure 8 presents data and theoretical results for the quasielastic, elastic, and inelastic processes at $E_{lab} = 46$ MeV. As earlier commented, the "elastic" scattering cross section has been defined as the sum of the contributions of the elastic process itself with the inelastic excitation of the 77-keV ^{197}Au state. Concerning the inelastic, we present results for the two groups composed by the 269-keV $3/2^+$ and 279-keV $5/2^+$ states, and by the 502-keV $5/2^+$ and 547-keV $7/2^+$ states, and also by the respective sum for all these states. We point out that, due to its very low excitation energies, there are not much data in the literature for ^{197}Au inelastic excitation from heavy-ion collisions. Our CRC results are in quite good agreement with the experimental data for all channels. We emphasize that the contamination of the experimental elastic and inelastic cross sections due to the one-neutron transfer is negligible. As can be observed in Fig. 8(a), the elastic scattering cross section becomes different from the Rutherford one at about 40°, which is a much more forward angle compared

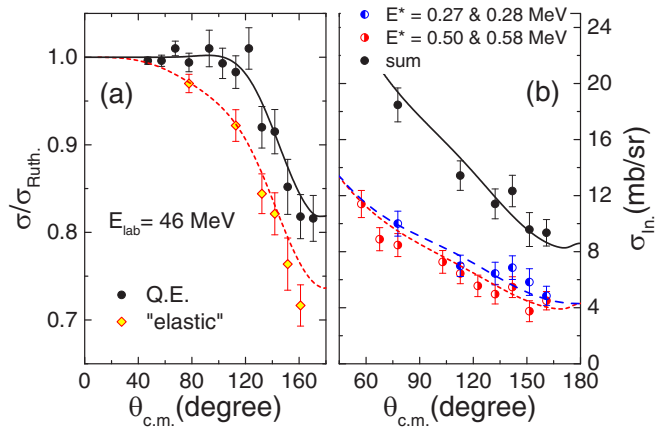

FIG. 8. Experimental angular distributions for (a) elastic and quasielastic scattering and (b) inelastic excitation of two groups of excited states and also for the respective sum. The lines in the figure represent the results of the CRC calculations.

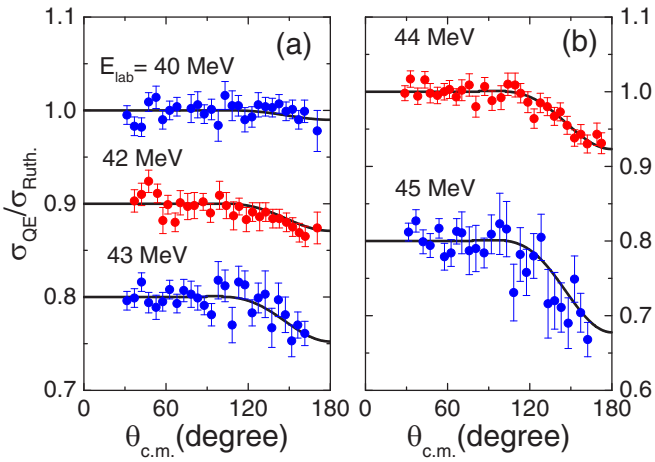

FIG. 9. Experimental angular distributions and corresponding CRC results for the quasielastic scattering in several bombarding energies. To avoid superposition of data, some angular distributions have been displaced by constant values.

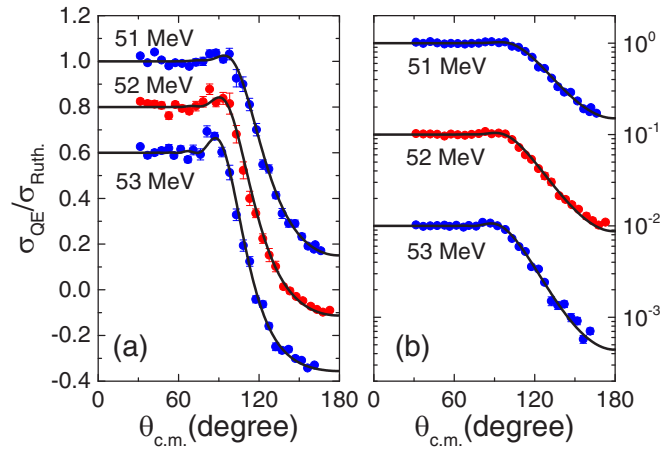

FIG. 11. Experimental and theoretical quasielastic scattering angular distributions in several bombarding energies, in linear (a) and logarithmic (b) scales. To avoid superposition, the cross sections for some angular distributions have been displaced (linear scale) or divided (logarithmic scale) by constant values.

to that ($\theta_{\text{c.m.}} \approx 100^\circ$) obtained under the same condition for the quasielastic process. This behavior arises from the long-range Coulomb excitation that transfers flux from the elastic scattering to inelastic excitation, without altering significantly the quasielastic cross section. Similar phenomenon was also observed in the elastic scattering for other systems due to the inelastic Coulomb excitation of very deformed nuclei with low-lying excitation energies [31]. Other mechanisms related to the breakup can also produce similar effects on the elastic scattering cross section (see, e.g., Refs. [31,32]).

Figures 9 and 10 present data and theoretical CRC results for the quasielastic process in several energies below (one slightly above) the barrier. Some angular distributions have been displaced by constant values to avoid superposition of data. The theoretical calculations are in quite good agreement with the data.

Figures 11, 12, and 13 shows quasielastic results for several energies above the barrier. Panels (a) and (b) of each of these figures present linear and logarithmic scales, respectively. Again, there is a quite good agreement between theory and experiment.

As already mentioned, for high energies it was also possible to obtain experimental estimate of cross sections for the elastic process by fitting peaks in the spectra. Figure 14 presents results for the elastic and quasielastic processes at $E_{lab} = 61$ MeV, in linear [Fig. 14(a)] and logarithmic [Fig. 14(b)] scales. The theoretical cross sections are in good agreement with the data for both processes.

B. Transfer reactions

We have detected ^{9}Be nuclei in the $\Delta E - E_K$ spectra (see, e.g., Fig. 2) that we associate to the one-proton stripping transfer and breakup processes: $^{10}\text{B} + ^{197}\text{Au} \rightarrow {}^{9}\text{Be} + {}^{198}\text{Hg}$ ($Q \approx 0.52$ MeV for the g.s.) and $^{10}\text{B} + ^{197}\text{Au} \rightarrow {}^{9}\text{Be} + {}^{197}\text{Au}$ + proton. The occurrence of breakup is deduced from considerations of energy. In fact, using the energy calibration of these spectra we verified that, in the case of transfer,

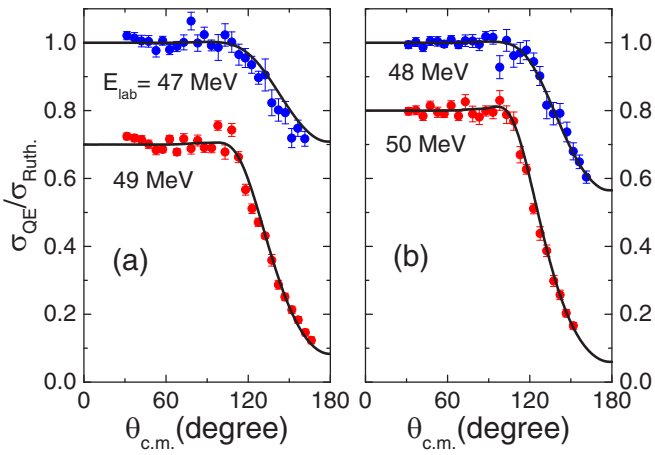

FIG. 10. The same as Fig. 9, for other energies.

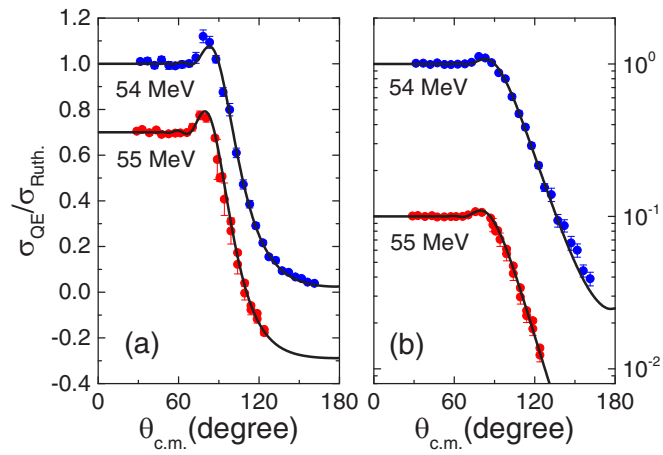

FIG. 12. The same as Fig. 11, for other energies.

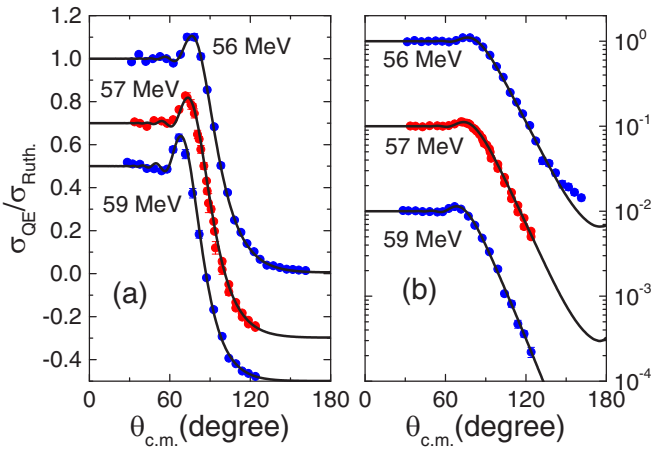

FIG. 13. The same as Fig. 11, for other energies.

the ^{9}Be detection would occur with Q values in the region of $-12.5 \leqslant Q \leqslant -4.5$ MeV. By energy conservation, the Q values implicate that ^{9}Be, ^{198}Hg, or even both nuclei should be found in excited states. However, the binding energy of the ^{198}Hg (proton + ^{197}Au) is only about 7.1 MeV, and the binding energy of the ^{9}Be (neutron + ^{8}Be) is about 1.6 MeV. Therefore, as illustrated in Fig. 2, part of the detected ^{9}Be nuclei should be associated to the proton stripping transfer and the other part should be related to the breakup reaction $^{10}\text{B} \rightarrow {}^{9}\text{Be} + \text{proton}$ populating the continuum.

Clearly, a realistic theoretical approach treating explicitly all these possibilities is quite complicated and beyond the scope of the present work. In order to describe this process through a quite simplified model, we considered just a schematic proton stripping transfer to a single ^{198}Hg level with excitation energy of $E^* = 6.5$ MeV. We have not used the average experimental value of $E^* = 8.5$ MeV because this energy would be enough to break the ^{198}Hg. In our schematic

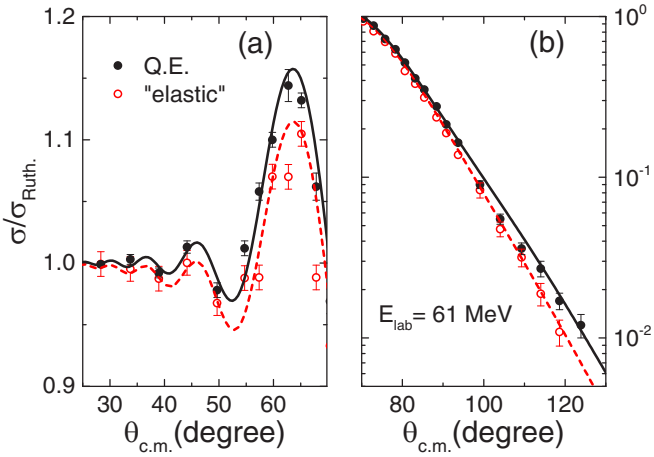

FIG. 14. Experimental and theoretical quasielastic and elastic scattering angular distributions at $E_{lab} = 61$ MeV, in linear (a) and logarithmic (b) scales.

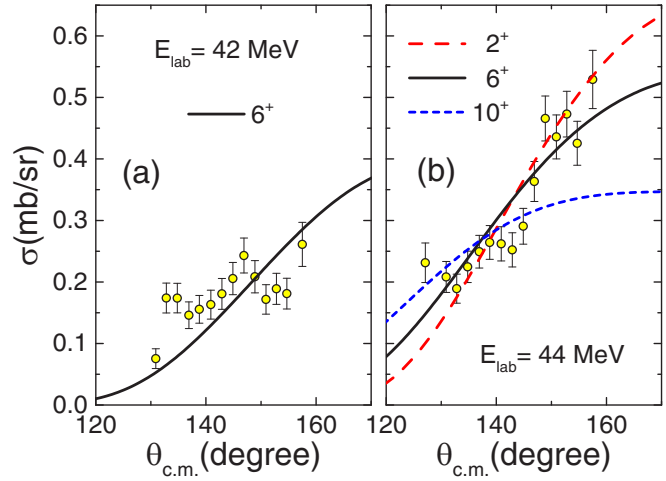

FIG. 15. Angular distributions related to the detection of ^{9}Be, at $E_{lab} = 42$ and 44 MeV. The theoretical results were obtained with schematic CRC calculations of one-proton stripping transfer (see text for details).

CRC calculation, we varied the spin of the ^{198}Hg excited state to check its effect on the shape of the angular distribution.

Data related to the ^{9}Be detection at $E_{lab} = 42$ and 44 MeV are shown in Fig. 15. In Fig. 15(b), we present theoretical results for the proton transfer angular distribution only for three different spins chosen as example. The corresponding spectroscopy factors were adjusted to fit the data. The shape of the experimental distribution at 44 MeV is reasonably reproduced using spin 6^+. The same spin also provides a reasonable description of the data at 42 MeV.

Figure 16 shows data for one-neutron pickup transfer in several bombarding energies, for the region of excitation energy of $0 \leqslant E^* \leqslant 1.8$ MeV. Since ^{11}B does not have excited states in this region, the excitation must be related to the ^{196}Au nucleus. There are a quite large number of ^{196}Au levels

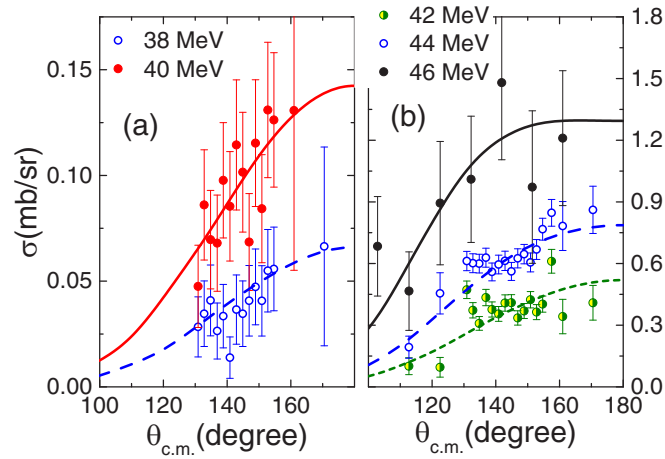

FIG. 16. Angular distributions for one-neutron pickup transfer in several bombarding energies. The data correspond to the region of ^{196}Au excitation energy of $0 \leqslant E^* \leqslant 1.8$ MeV.

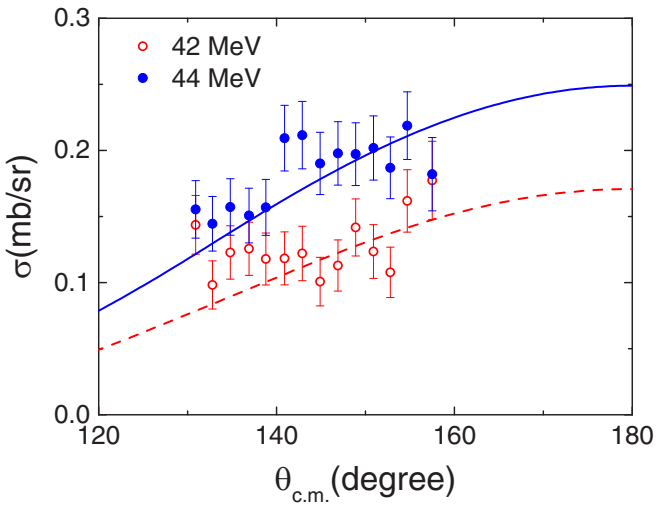

FIG. 17. Experimental and theoretical angular distributions for one-neutron pickup transfer, in the region of excitation energy of $4 \leqslant E^* \leqslant 8$ MeV.

in this excitation energy region, which makes impracticable to perform CRC calculations considering all possibilities. Thus, we have again performed schematic calculations of one-neutron transfer, considering one single ^{196}Au state with excitation energy of 0.9 MeV (average excitation energy of the data). The corresponding results are shown through the lines in Fig. 16. Similar results were obtained for the region $4 \leqslant E^* \leqslant 8$ MeV, which are presented in Fig. 17.

Table II presents the total (integrated over angle) cross sections of our theoretical calculations for the transfer processes. We mention that the transfer couplings do not result in significant contributions to the cross sections of the other channels: quasielastic, elastic, and inelastic excitations.

C. Breakup process

The ^{10}B breakup thresholds in the ^{6}Li $+\alpha$ and ^{9}Be $+p$ partitions are 4.461 and 6.586 MeV, respectively. Because these energies are lower than typical binding energies of strongly bound nuclei, it would be expected that the breakup channel could have an effect in the reactions induced by ^{10}B projectiles. In a previous publication, it was shown that the effect of the couplings to the continuum on the elastic-scattering cross sections for the ^{10}B $+$ ^{120}Sn measured at energies around the Coulomb barrier is very small [20]. Even so, for completeness, we have performed continuum-discretized coupled-channels (CDCC) calculations using the FRESCO code [25] to check whether this is also the case for the ^{10}B $+$ ^{197}Au reaction. Calculations have been performed for the highest measured incident energy $E_{lab} = 61$ MeV and the two energies in which ^{9}Be has been detected ($E_{lab} = 42$ and 44 MeV).

We have used the two-body cluster models referred above, ^{6}Li $+\alpha$ and ^{9}Be $+p$. The corresponding binding potentials were calculated using the SPP model. For the optical potentials between the projectile fragments and the target, the SPP is also adopted for the real part of the interaction. The imaginary potential is the same as assumed in the CRC calculations; i.e., the SPP has been multiplied by $N_I = 0.3$. We have considered the ground state and the first bound excited states of the projectile. However, the excitation of the target is not included in the CDCC calculations. Therefore, we refer the corresponding calculated cross sections to *elastic breakup* (EBU). The ^{6}Li $+\alpha$ and ^{9}Be $+p$ continuum states were discretized into energy bins, evenly spaced in the asymptotic momentum k, and up to a maximum excitation energy of 15 MeV for $E_{lab} = 61$ MeV and 5 MeV for $E_{lab} = 42$ and 44 MeV. We included s, p, and d waves for the two-body relative orbital angular momentum.

For both considered partitions, the results show that the EBU cross section is lower than 0.5 mb for $E_{lab} = 61$ MeV and is practically negligible for $E_{lab} = 42$ and 44 MeV, being of about 10^{-2} and 10^{-3} mb, respectively. The calculated EBU cross sections for $E_{lab} = 42$ and 44 MeV are much lower than the experimental values obtained from the detection of ^{9}Be (see Table II). It is worth mentioning that adopting $N_I = 0.78$, which is the value often used to describe the elastic scattering of many systems in wide mass and energy ranges [33], decreases even more the EBU cross sections. We believe that part of the observed discrepancy between data and theory can be related to the fact that other processes, such as the breakup accompanied by the excitation of the target, or the transfer or fusion of one of the breakup fragments to the target, are not been included in the CDCC calculations. These processes are referred to *nonelastic breakup* (NEB) in Ref. [34], where it is shown that the NEB cross sections can be much larger than the EBU for systems involving ^{6}Li on several targets. However, the evaluation of NEB is not a simple task and out of the scope of this paper.

TABLE II. Total (integrated) cross sections (in mb) obtained with our theoretical calculations for the neutron (in two different regions of excitation energy) and proton transfer (plus breakup) processes.

E_{lab}(MeV)	$0 \leqslant E^* \leqslant 1.8$ MeV	$4 \leqslant E^* \leqslant 8$ MeV	Proton
38	0.15		
40	0.34		
42	1.3	0.39	0.46
44	2.4	0.61	0.98
46	5.0		

IV. DISCUSSION AND SUMMARY

In this paper, we have presented a wide data set obtained for ^{10}B $+$ ^{197}Au at near-barrier energies, through measurements that involved the detection of different channels. The fit of the quasielastic, elastic scattering, and inelastic excitation data was performed through CRC calculations with only two energy-independent adjustable parameters. A quite good agreement between theory and experiment was obtained with the following best-fit values: $N_I = 0.30$ for the imaginary part of the optical potential and $V_0 = 6$ MeV for the spin-orbit interaction.

Because of the small values of excitation energies, the inelastic excitation of the low-lying ^{197}Au states removes

significant amount of flux from the elastic channel in both energy regions: below and above the barrier. We have obtained a good overall description of the experimental one-neutron pickup transfer cross sections through schematic CRC calculations involving only one single ^{196}Au state.

Events involving the detection of the ^{9}Be nucleus were observed in our experiments. The range of kinetic energy of the detected nuclei indicates that they can be produced in different processes: transfer $^{10}\mathrm{B} + {}^{197}\mathrm{Au} \rightarrow {}^{9}\mathrm{Be} + {}^{198}\mathrm{Hg}$, and breakup $^{10}\mathrm{B} + {}^{197}\mathrm{Au} \rightarrow {}^{9}\mathrm{Be} + {}^{197}\mathrm{Au} + \text{proton}$. Possibly, the ^{9}Be nuclei can also breakup in $^{9}\mathrm{Be} \rightarrow \text{neutron} + {}^{8}\mathrm{Be}$, where the ^{8}Be breaks again in two α's. In fact, we have detected α particles in our spectra. However, these particles can originate from several different processes. To distinguish among them, it would be necessary to perform measurements in temporal coincidence. We also point out that although the $^{6}\mathrm{Li} + \alpha$ is energetically the most favorable partition for the breakup of ^{10}B ($Q \approx -4.5$ MeV), we have not observed ^{6}Li in the present experiment. Similar behavior has been reported in the case of $^{10}\mathrm{B} + {}^{159}\mathrm{Tb}$ [22], where γ rays coming from the capture of α particle by the target were not detected.

We have performed CDCC calculations for three incident energies considering that the ^{10}B projectile can break up into two different partitions: $^{6}\mathrm{Li} + \alpha$ and $^{9}\mathrm{Be} + p$. Even for the highest incident energy ($E_{Lab} = 61$ MeV), the calculated EBU cross section is lower than 0.5 mb. For $E_{Lab} = 42$ and 44 MeV, the EBU is much smaller than the experimental cross sections obtained from the yields of the observed ^{9}Be nucleus. A significant part of the missing cross sections can be associated to the NEB processes.

During the experimental campaign at TANDAR, we have also performed simultaneous measurements of fusion. The main results are given in a separated paper [23].

ACKNOWLEDGMENTS

This work was partially supported by Fundação de Amparo à Pesquisa do Estado de São Paulo (FAPESP) Proc. No. 2018/09998-8 and No. 2017/05660-0, by the Conselho Nacional de Desenvolvimento Científico e Tecnológico (CNPq), Proc. No. 407096/2017-5 and No. 306433/2017-6, project INCT-FNA Proc. No. 464898/2014-5, and by the Conselho de Aperfeiçoamento de Pessoal de Nível Superior (CAPES). This work was also partially supported by the Ministry of Science, Innovation and Universities of Spain, through the Project No. PGC2018-096994-B-C21, by the Spanish Ministry of Economy and Competitiveness, the European Regional Development Fund (FEDER), under Project No. FIS2017-88410-P, and by the European Union's Horizon 2020 research and innovation program, under Grant Agreement No. 654002. Argentinean authors acknowledge Grants No. PIP00786CO (CONICET) and No. PICT-2017-4088 from FONCyT. A.A., M.A.C., D.H., and A.J.P. are fellows of CONICET.

[1] R. B. Wiringa, Rev. Mod. Phys. **65**, 231 (1993).
[2] N. Takigawa and K. Washiyama, *Bulk Properties of Nuclei* (Springer, Tokyo, 2017), p. 13.
[3] A. Kumar, R. Kanungo, A. Calci, P. Navratil, A. Sanetullaev, M. Alcorta, V. Bildstein, G. Christian, B. Davids, J. Dohet-Eraly, J. Fallis, A. T. Gallant, G. Hackman, B. Hadinia, G. Hupin, S. Ishimoto, R. Krucken, A. T. Laffoley, J. Lighthall, D. Miller, S. Quaglioni, J. S. Randhawa, E. T. Rand, A. Rojas, R. Roth, A. Shotter, J. Tanaka, I. Tanihata, and C. Unsworth, Phys. Rev. Lett. **118**, 262502 (2017).
[4] A. Yoshida, C. Signorini, T. Fukuda, Y. Watanabe, N. Aoi, M. Hirari, M. Ishihara, H. Kobinata, Y. Mizoi, L. Mueller, N. Nagashima, J. Nakano, T. Nomura, Y. H. Pu, and F. Scarlassara, Phys. Lett. B **389**, 457 (1996).
[5] J. J. Kolata, V. Guimarães, D. Peterson, P. Santi, R. White-Stevens, P. A. DeYoung, G. F. Peaslee, B. Hughey, B. Atalla, M. Kern, P. L. Jolivette, J. A. Zimmerman, M. Y. Lee, F. D. Becchetti, E. F. Aguilera, E. Martinez-Quiroz, and J. D. Hinnefeld, Phys. Rev. Lett. **81**, 4580 (1998).
[6] M. Trotta, J. L. Sida, N. Alamanos, A. Andreyev, F. Auger, D. L. Balabanski, C. Borcea, N. Coulier, A. Drouart, D. J. C. Durand, G. Georgiev, A. Gillibert, J. D. Hinnefeld, M. Huyse, C. Jouanne, V. Lapoux, A. Lepine, A. Lumbroso, F. Marie, A. Musumarra, G. Neyens, S. Ottini, R. Raabe, S. Ternier, P. VanDuppen, K. Vyvey, C. Volant, and R. Wolski, Phys. Rev. Lett. **84**, 2342 (2000).
[7] K. Wimmer, J. Phys. G: Nucl. Part. Phys. **45**, 033002 (2018).
[8] U. Umbelino, K. C. C. Pires, R. Lichtenthäler, V. Scarduelli, G. A. Scotton, A. Lépine-Szily, V. Guimarães, J. Lubian, B. Paes, J. L. Ferreira, M. A. G. Alvarez, J. M. B. Shorto, S. Appannababu, M. Assunção, R. P. Condori, and V. Morcelle, Phys. Rev. C **99**, 064617 (2019).
[9] S. Appannababu, R. Lichtenthaler, M. A. G. Alvarez, M. Rodriguez-Gallardo, A. Lepine-Szily, K. C. C. Pires, O. C. B. Santos, U. U. Silva, P. N. de Faria, V. Guimaraes, E. O. N. Zevallos, V. Scarduelli, M. Assuncao, J. M. B. Shorto, A. Barioni, J. Alcantara-Nunez, and V. Morcelle, Phys. Rev. C **99**, 014601 (2019).
[10] M. Mazzocco, C. Signorini, M. Romoli, A. D. Francesco, M. D. Pietro, E. Vardaci, K. Yoshida, A. Yoshida, R. Bonetti, A. D. Rosa, T. Glodariu, A. Guglielmetti, G. Inglima, M. L. Commara, B. Martin, D. Pierroutsakou, M. Sandoli, and F. Soramel, Eur. Phys. J. A **28**, 295 (2006).
[11] A. Di Pietro, G. Randisi, V. Scuderi, L. Acosta, F. Amorini, M. J. G. Borge, P. Figuera, M. Fisichella, L. M. Fraile, J. Gomez-Camacho, H. Jeppesen, M. Lattuada, I. Martel, M. Milin, A. Musumarra, M. Papa, M. G. Pellegriti, F. Perez-Bernal, R. Raabe, F. Rizzo, D. Santonocito, G. Scalia, O. Tengblad, D. Torresi, A. M. Vidal, D. Voulot, F. Wenander, and M. Zadro, Phys. Rev. Lett. **105**, 022701 (2010).
[12] V. Pesudo, M. J. G. Borge, A. M. Moro, J. A. Lay, E. Nácher, J. Gómez-Camacho, O. Tengblad, L. Acosta, M. Alcorta, M. A. G. Alvarez, C. Andreoiu, P. C. Bender *et al.*, Phys. Rev. Lett. **118**, 152502 (2017).
[13] V. A. B. Zagatto, J. Lubian, L. R. Gasques, M. A. G. Alvarez, L. C. Chamon, J. R. B. Oliveira, J. A. Alcantara-Nunez, N. H. Medina, V. Scarduelli, A. Freitas, I. Padron, E. S. Rossi, and J. M. B. Shorto, Phys. Rev. C **95**, 064614 (2017).
[14] A. Kundu, S. Santra, A. Pal, D. Chattopadhyay, R. Tripathi, B. J. Roy, T. N. Nag, B. K. Nayak, A. Saxena, and S. Kailas, Phys. Rev. C **95**, 034615 (2017).

[15] A. Arazi, J. Casal, M. Rodriguez-Gallardo, J. M. Arias, R. Lichtenthaler Filho, D. Abriola, O. A. Capurro, M. A. Cardona, P. F. F. Carnelli, E. de Barbara, J. Fernandez Niello, J. M. Figueira, L. Fimiani, D. Hojman, G. V. Marti, D. Martinez Heimman, and A. J. Pacheco, Phys. Rev. C **97**, 044609 (2018).
[16] R. Rafiei, R. du Rietz, D. H. Luong, D. J. Hinde, M. Dasgupta, M. Evers, and A. Diaz-Torres, Phys. Rev. C **81**, 024601 (2010).
[17] D. H. Luong, M. Dasgupta, D. J. Hinde, R. du Rietz, R. Rafiei, C. J. Lin, M. Evers, and A. Diaz-Torres, Phys. Lett. B **695**, 105 (2011).
[18] S. Kalkal, E. C. Simpson, D. H. Luong, K. J. Cook, M. Dasgupta, D. J. Hinde, I. P. Carter, D. Y. Jeung, G. Mohanto, C. S. Palshetkar, E. Prasad *et al.*, Phys. Rev. C **93**, 044605 (2016).
[19] L. R. Gasques, A. S. Freitas, L. C. Chamon, J. R. B. Oliveira, N. H. Medina, V. Scarduelli, E. S. RossiJr., M. A. G. Alvarez, V. A. B. Zagatto, J. Lubian, G. P. A. Nobre, I. Padron, and B. V. Carlson, Phys. Rev. C **97**, 034629 (2018).
[20] M. A. G. Alvarez, M. Rodrígues-Gallardo, L. R. Gasques, L. C. Chamon, J. R. B. Oliveira, V. Scarduelli, A. S. Freitas, E. S. Rossi, V. A. B. Zagatto, J. Rangel, J. Lubian, and I. Padron, Phys. Rev. C **98**, 024621 (2018).
[21] L. R. Gasques, D. J. Hinde, M. Dasgupta, A. Mukherjee, and R. G. Thomas, Phys. Rev. C **79**, 034605 (2009).
[22] A. Mukherjee, R. Subinit, M. K. Pradhan, M. S. Sarkar, P. Basu, B. Dasmahapatra, T. Bhattacharya, S. Bhattacharya, S. K. Basu, A. Chatterjee, V. Tripathi, and S. Kailas, Phys. Lett. B **636**, 91 (2006).
[23] M. Aversa, D. Abriola, M. A. G. Alvarez, A. Arazi, M. A. Cardona, L. C. Chamon, E. de Barbará, J. de Jesús, J. P. Fernández-García, L. R. Gasques, D. Hojman, A. Lépine-Szily, G. V. Martí, A. J. Pacheco, V. Scarduelli, and V. A. B. Zagatto, Phys. Rev. C **101**, 044601 (2020).
[24] D. Dell'Aquila, I. Lombardo, G. Verde, M. Vigilante, G. Ausanio, A. Ordine, M. Miranda, M. D. Luca, R. Alba, L. Augey, S. Barlini, E. Bonnet, B. Borderie *et al.*, Nucl. Instrum. Methods A **877**, 227 (2018).
[25] I. J. Thompson, Comput. Phys. Rep. **7**, 167 (1988).
[26] L. C. Chamon, B. V. Carlson, L. R. Gasques, D. Pereira, C. De Conti, M. A. G. Alvarez, M. S. Hussein, M. A. Cândido Ribeiro, E. S. Rossi, Jr., and C. P. Silva, Phys. Rev. C **66**, 014610 (2002).
[27] X. Huang and C. Zhou, Nucl. Data Sheets **104**, 283 (2005).
[28] W. J. Vermeer, R. K. Bhalla, and A. R. Poletti, Phys. Rev. C **28**, 432 (1983).
[29] L. C. Chamon and B. V. Carlson, Nucl. Phys. A **846**, 1 (2010).
[30] P. Raghavan, At. Data Nucl. Data Tables **42**, 189 (1989).
[31] N. Keeley, K. W. Kemper, and K. Rusek, Eur. Phys. J. A **50**, 145 (2014).
[32] J. P. Fernández-García, M. Cubero, L. Acosta, M. Alcorta, M. A. G. Alvarez, M. J. G. Borge, L. Buchmann, C. A. Diget, H. A. Falou, B. Fulton, H. O. U. Fynbo, D. Galaviz *et al.*, Phys. Rev. C **92**, 044608 (2015).
[33] M. A. G. Alvarez, L. C. Chamon, M. S. Hussein, D. Pereira, L. R. Gasques, E. S. Rossi, Jr., and C. P. Silva, Nucl. Phys. A **723**, 93 (2003).
[34] J. Lei and A. M. Moro, Phys. Rev. C **92**, 044616 (2015).